Effect of microstructure and chemical composition on subcritical crack growth in SiC-based fiber tows

Stephane Mazerat, Rene Pailler

Effect of microstructure and chemical composition on subcritical crack growth in SiC-based fiber tows

S. Mazerat, R. Pailler*

Univ. Bordeaux, CNRS, CEA, SAFRAN CERAMICS, LCTS, UMR 5801, F-33600 Pessac, France
* Corresponding author. Tel +33 5 56844733; Fax +33 5 56841225. E-mail address: pailler@lcts.u-bordeaux.fr

Abstract

SiC-based fibers, a key component for the reinforcement of thermostructural ceramic matrix composites, are subjected to subcritical crack growth (SCG) causing their delayed failure. Stress exponents <10 were reported for various fiber types, standing out from other types of ceramic or glass. The continuum of silicon oxycarbide (SiCO) and carbon free phases is suspected to govern the environmentally assisted crack growth phenomenon, highlighted by relationships between SCG parameters and oxygen or carbon free contents. Metallic heteroelements (Ti or Zr, found in Tyranno® fibers) play a critical role on this sensitivity as well. The existence of 2 distinct groups of fiber types, possibly associated to different SCG mechanisms, is discussed.

Keywords

SiC fiber ; Slow crack growth ; Static fatigue ; Lifetime prediction parameter

1. Introduction

Owning to their high specific strength at elevated temperature, creep resistance, low thermal expansion, high thermal conductivity, chemical inertness and weaving suitability, SiC-based fibers have become a strategic component for the long reinforcement of SiC/SiC Ceramic Matrix Composite (CMC), for application in power plant, jet engine or sport automotive [1,2]. Like many oxide [3-7] or non oxide [8-11] brittle materials, these fibers are however subjected to a thermally activated delayed failure under the combined effect of environment and subcritical stress (for temperature below the creep threshold <1100 °C [12]). A power law is commonly accepted to predict such lifetime (t_f), relating the stress intensity factor (K_I) to crack growth velocity (V) (Eq. (1)), transformed and simplified into Eq. (2) using the fracture mechanics law.

$$V = \frac{da}{dt} = V^* \left(\frac{K_I}{K_{IC}} \right)^n \quad (1)$$

$$t_f = A\sigma_{app}^{-n} \quad (2)$$

Where a is the crack size, K_{IC} the toughness, n the stress corrosion susceptibility coefficient, here referred as stress exponent, and σ_{app} the stress. V^* and A are environmental constants following an Arrhenius law (Eq. (3)), with Ea_{SCG} the slow crack growth (SCG) apparent activation energy and A_0 the pre-exponential constant.

$$A = A_0 e^{\frac{Ea_{SCG}}{RT}} \quad (3)$$

Stress exponent ranging from 5 to 10 were assessed by static fatigue on SiC bundles [13-15], below the 10-400 range reported on classical oxide [16,17] or covalent non oxide [8,18-20] ceramics. A low stress exponent is often associated with a higher susceptibility to SCG (and vice versa) and suggests that the corrosion-environmental effect is the dominant factor, instead of stress. Substrate properties are likely to have a large influence on this environmentally assisted failure. If the chemical attack of strained bonds at crack tip is assumed for glass or oxide ceramics [21], carbon free oxidation or volume expansion at crack lips was proposed to explain the same on Hi-Nicalon and Hi-Nicalon-S SiC fibers [22].

In the present work, SCG parameters for various SiC-based fiber types were gathered. The understanding of how they compare to properties (mechanical, chemical or microstructural) has not been addressed yet. The results provide guidance for the selection of adequate fiber type to warrant application needs. Indeed, one of the key challenge for CMC development remains this so-called design on purpose strategy: tailored reinforcement type (high or low n) to suit the local stress or environmental condition and their versatility.

2 Material and method

Three generations of SiC-based fibers are commercially available, synthesized by the conversion of polycarbosilane (Nippon Carbon Co. Ltd. under the trade name Nicalon®), or derivate containing a small amount of organometallic (UBE Industries Ltd. named Tyranno®). The first-generation fibers are composed of SiC grains in nanometer range embedded in a silicon oxycarbide phase (SiCO) and free aromatic carbon (C_{free}) as basic structural units [23,24]. Second generation fibers are however electron beam cured, hence oxygen free, and contain excess of carbon inhibiting SiC grain growth, also in nanometer range. In the other hand, near stoichiometric third-generation fibers are constituted of coarser SiC grains (>50 nm) and display good stability at high temperature. In this study, 4 first-generation fibers are reported: Nicalon® NL207, Tyranno® Grade S (titanium doped), referred as TS, Tyranno® Lox-M (titanium doped) and Tyranno® ZMI (zirconium doped). Two different batches of TS tows were characterized. The first TS yarn batch contained 1600 fibers with 8.5 µm average diameter, the second one 800 fibers with 11 µm mean diameter, respectively called TS and TS11.

Second-generation Hi-Nicalon (Hi-Ni) and third-generation Hi-Nicalon Type S (Hi-Ni-S), with distinct microstructure and composition, complete the study. Their chemical composition and microstructure are summarized in Table 1.

Static fatigue tests were carried out on fiber bundles with hot grips technique described elsewhere [15,25,26]. Sized bundles were glued with alumina based thermostructural cement (Ceramabond 503, Polytec PI) in alumina grips and cured at 370 °C for 2 hours. Probe was installed in a vertical resistive furnace and a dead weight (w_t Eq. (4), where γ is the fraction of initially broken filament) suspended to lower grip. The time before a probe had failed thereby defines its lifetime.

$$\sigma_\gamma = \frac{w_t}{S_t(1-\gamma)} \tag{4}$$

Where σ_γ is the stress applied to the tow and S_t its total section.

3. Results

Some properties for the 6 fiber types, brought to 7 considering the 2 Grade S batches, are gathered in Table 1. Toughness, extracted from fractographic analysis, coherently evolves with the silicon oxycarbide phase, ranging from 1 to 1.2 MPa $m^{1/2}$ when present on first-generation fibers and >1.5 MPa $m^{1/2}$ when absent. The elastic modulus, following a mixture rule associated to the volume fraction of each phase [27], is another good indicator of the microstructure. Tyranno® SiCO fibers, with a higher carbon free content, show a Young modulus and a toughness below the NL207. This tendency is exacerbated on Grade S fibers due to the high oxygen content and associated volume of SiCO phase, exceeding the 10-13 at.% range of NL207, Lox-M or ZMI. Their β-SiC grain size is also lower. Whilst showing a higher oxygen content, TS11 displays properties similar to TS. Hi-Ni fiber type is oxygen free and contain about 16 at.% carbon free, similarly to NL207 though with a higher percolation state [27]. The same comment applies to ZMI compared to Lox-M or TS. The absence of silicon oxycarbide (SiCO) phase has a remarkable impact on the Young modulus and toughness of these second and third generation fibers. Based on these properties, Hi-Ni-S and in a lower extend Hi-Ni, would be expected to show distinct behavior in static fatigue condition when compared to first-generation fiber types.

	NL207	TS	TS11	Lox-M	ZMI	Hi-Ni	Hi-Ni-S
Si	38.6	31.8	31.6	35.4	35.5	41.9	48.2
C	48.6	48.1	41.7	53.3	54.3	57.2	50.8
O (at.%)	12.8	19.4	26.0	10.4	10.0	0.9	1.0
other	-	(Ti) 0.7	(Ti) 0.7	(Ti) 0.9	(Zr) 0.2	-	-
C_{free}	16.4	26.0	23.0	23.1	23.9	15.8	3.1
Grain size (nm)	1.9	1.2	1.2	1.9	2.2	5.0	50
K_{IC} (MPa $m^{1/2}$)	1.20	1.11	1.12	1.11	1.01	1.66	1.86
E (GPa)	210	180	180	200	200	300	410
n	7.3	5.0	5.8	4.9	9.1	8.4	7.2
$A_{500\,°C}$ (MPa s^n)	2.0×10^{27}	2.4×10^{20}	9.4×10^{22}	4.3×10^{20}	2.1×10^{33}	1.5×10^{30}	5.7×10^{28}
$A_{600\,°C}$ (MPa s^n)	1.7×10^{26}	4.1×10^{19}	1.6×10^{22}	3.2×10^{19}	9.8×10^{31}	5.8×10^{28}	2.5×10^{27}
$A_{700\,°C}$ (MPa s^n)	2.4×10^{25}	1.0×10^{19}	3.7×10^{21}	4.1×10^{18}	8.6×10^{30}	4.5×10^{27}	2.1×10^{26}
$A_{800\,°C}$ (MPa s^n)	5.0×10^{24}	3.3×10^{18}	1.2×10^{21}	7.6×10^{17}	1.2×10^{30}	5.5×10^{26}	2.7×10^{25}
Ea_{SCG} (kJ mol^{-1})	140	100	100	150	170	180	170
A_0 (MPa s^n)	9.8×10^{17}	5.8×10^{13}	1.4×10^{16}	6.1×10^{10}	5.1×10^{21}	8.4×10^{17}	7.3×10^{16}

Table 1: Composition, physical and mechanical properties completed with SCG parameters for the different SiC-based fibers.

Slow crack growth coefficients are also given in Table 1. The values for stress exponent differ markedly from type to type, ranging from 5 (Lox-M) to 9 (ZMI). On Hi-Ni-S, 7.2 [26] and 8.2 [14] stress exponents were reported in literature. Albeit assessed on distinct probes (length scale, preparation) and temperature range, these are however not expected to have such impact on prediction parameters. Environmental coefficients (A), as well as pre-exponential A_0, are strongly related to the stress exponent making direct comparison difficult. Apparent activation energies for SCG under ambient atmosphere and intermediate temperatures ranges from 100 kJ mol^{-1} (on the high oxygen containing TS and TS11 fibers) to 180 kJ mol^{-1} on Hi-Nicalon, itself close to Hi-Ni-S and ZMI types both lying at 170 kJ mol^{-1}. NL207 and Lox-M are intermediate with 140 and 150 kJ mol^{-1} respectively [15]. A first observation can be drawn: despite 10 at.% oxygen, Lox-M and ZMI types show a drastic different behavior, mostly pointed by the stress exponent. Moreover, although being near stoichiometric (absence of SiCO and C_{free} phases) with pertinent properties (Table 1), Hi-Ni-S bundles show SCG parameters comparable with other fiber types. Thence, no obvious relationship between these coefficients and substrate properties appear. Endurance diagrams, showing the predicted lifetime for different applied stresses, indicate that lifetimes of several years would be expected for tow under low stresses (<300 MPa) (Fig. 1). This statement implicitly considers the model (Eq. (2)) can be extrapolated for such duration and no additional embrittlement mechanism is activated. Such diagram can argue the selection of a given reinforcement type. For instance, ZMI and Hi-Ni-S tows have markedly higher lifetime at 600 °C or 800 °C while Hi-Ni, though closer to Hi-Ni-S in terms of composition, show the lowest lifetimes for stresses >300 MPa. Other first-generation fibers are close to each other. This observation shows the stress exponent can not, by its own, indicate which fiber type should be preferred to match expected performances in terms of service life. The environmental coefficient (A) should as

well be considered, following a given evolution with temperature as illustrated by the Ea_{SCG} parameter. For temperatures below 600 °C, such ranking would indeed be different, more favorable for Hi-Ni. Microstructural, mechanical or chemical factors would likely explain these statements afterward discussed.

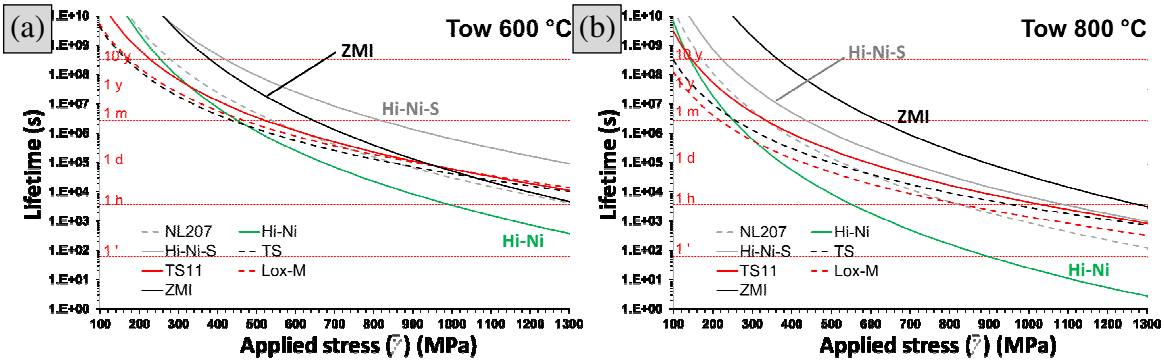

Fig. 1: Endurance diagram comparing the predicted median lifetime (Eq. (2)) for the different fiber types at (a). 600 °C and (b). 800 °C.

4. Discussion

The general trend to low stress exponents of these SiC based tows, compared to sintered SiC or glass samples commonly >20, must be emphases as indicative of strong sensitivity to thermo-chemical mechanism. A larger stress exponent could have been expected on Hi-Ni-S with regard to the larger grain size involved [19,28]. Several classification approaches are offered based on prediction parameters. The apparent activation energy would for instance distinguish 3 groups: 170-180 kJ mol^{-1} (Hi-Ni, Hi-Ni-S, ZMI), 140-150 kJ mol^{-1} (NL207, Lox-M) and 100 kJ mol^{-1} (TS, TS11) (Fig. 2). Stress exponent would alternatively distinguish the titanium doped fibers (n<6) from others (6<n<9). Relationship between the SCG parameters and some fiber characteristics (chemical composition or mechanical behavior) however points 2 families: the first one (①) gathering low oxygen or zirconium doped types, the second one (②) with higher (>10 at.%) oxygen content.

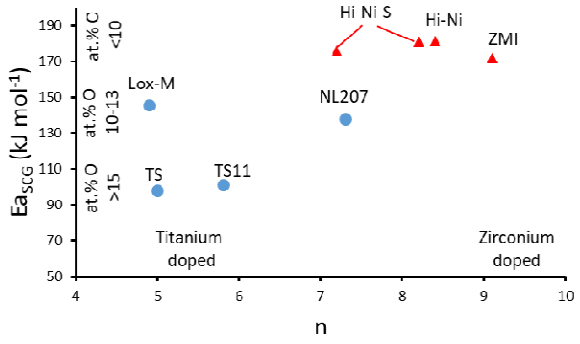

Fig. 2: Apparent SCG activation energy versus stress exponent for different SiC-based fiber types. Red triangles and blue dots indicate respectively families ① and ②.

The first justification for such classification originates from the relationship between stress exponent and carbon free content or Young's modulus (toughness shows similar trend): distinct linear trend. When the carbon free content increases, going together with a lower elastic modulus, the stress exponent increases on ①, whereas the opposite behavior is observed with ② (Fig. 3) in a better agreement with literature data [29]. The activation energy seems globally to increase when the oxygen content, thus the volume fraction of silicon oxycarbide phase, decreases (Fig. 4a). As indicated in result section, the environmental coefficient is strongly related to the stress exponent and thus hardly comparable. Elevated to the $1/n^{th}$ power these coefficients are more comparable and seems linearly related to n, both families combined (Fig. 4b). ZMI and Hi-Ni-S stand above this trend, indicative for their superior resistance to SCG (Fig 1).

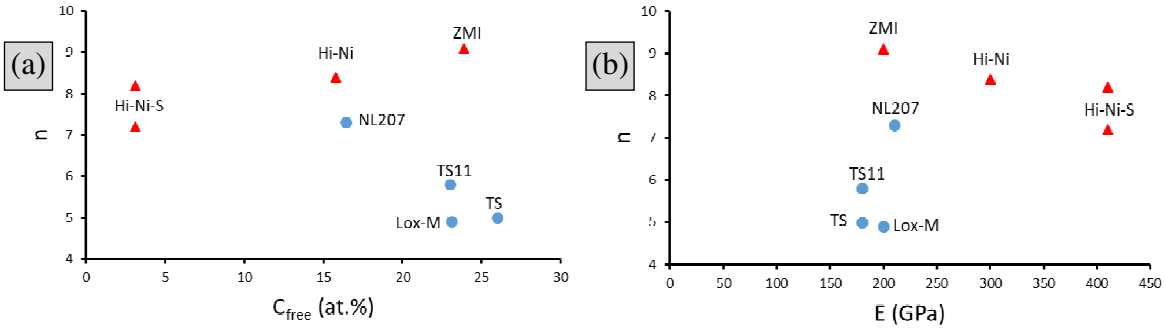

Fig. 3: Evolution of stress exponent with (a). carbon free content or (b). Young modulus.

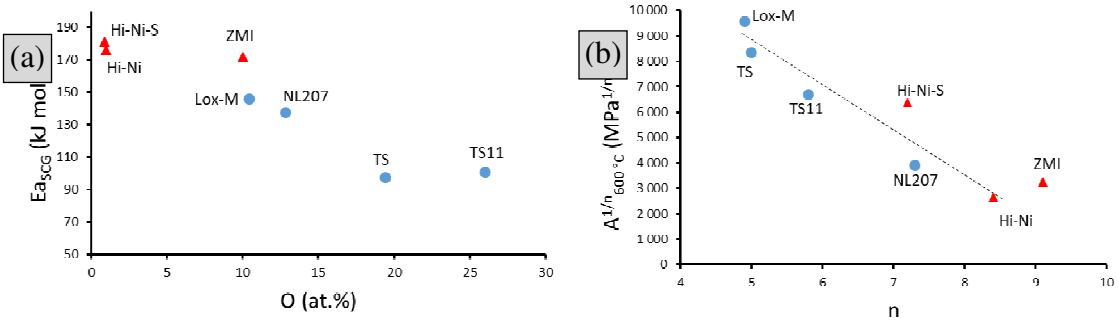

Fig. 4: Evolution of (a). apparent activation energy for SCG at intermediate temperature with oxygen content and (b). $A^{1/n}$ taken at 600 °C with stress exponent.

Emphasis should be placed upon the effect heteroelement type (Ti or Zr in Tyranno® fibers) seems to play on stress exponent. Although titanium and aluminum were respectively incorporated to preclude or foster β-SiC grain growth, zirconium-doped fibers development was chiefly motivated by improved corrosion, oxidation and heat resistance [30]. Classification of ZMI fiber with the oxygen free group (①) could hence be interpreted as follows: when zirconium-stabilized, the fiber is not subjected to stress corrosion of the silicon oxycarbide phase (absent in Hi-Ni and Hi-Ni-S); carbon free oxidation becomes the piloting factor (percolation related severity) with Ea_{SCG} about 170-180 kJ mol^{-1}. Titanium would however have a converse effect, enhancing the sensitivity to chemical attack thus lowering the stress exponent. Alternative fibers, not yet studied under static fatigue condition such as Lox-E (5 at.% O, Ti) or ZM (9 at.%O, Zr) etc… [27], would argue this explanation.

5. Conclusion

SiC-based filament tow are subjected to SCG mechanism causing their delayed failure, found to be strongly dependent on the fiber type. Fiber with low oxygen content (second or third generation) or zirconium stabilized, show a homogeneous activation energy and relatively high stress exponents. They are hence less sensitive to environmental chemical attack than a second group instead displaying high (>10 at.%) oxygen content with lower stress exponents and activation energies. Carbon free, oxygen content and metallic heteroelement were highlighted as major factors affecting the SCG rate and mechanism. If, for the former group, oxidation at flaw crack tip of carbon free (favored by its percolation state) was proposed, stress corrosion of the SiCO continuum phase is however suspected for the latter group. These findings would argue further development or selection of CMC continuous reinforcement for extended life applications. A better understanding of the stress accelerated chemical reaction leading to the crack growth seems prominent to further explain the here highlighted relationships.

Acknowledgements

The authors acknowledge the financial support of Safran Ceramics for this work.

References

[1] R. Naslain, Design, preparation and properties of non-oxide CMCs for application in engines and nuclear reactors: an overview, Comp. Sci. Tech. 64(2) (2004) 155−170.
doi: 10.1016/S0266-3538(03)00230-6

[2] Y. Katoh, L.L.Snead, Silicon carbide and its composites for nuclear applications – Historical overview, J. Nuclear Mater. 526 (2019) 151849.
doi: 10.1016/j.jnucmat.2019.151849

[3] S.M. Wiederhorn, L.H. Boltz, Stress corrosion and static fatigue of glass, J. Am. Ceram. Soc. 53(10) (1970) 543−548.
doi: 10.1111/j.1151-2916.1970.tb15962.x

[4] A.G. Evans, S.M. Wiederhorn, Proof testing of ceramic materials—an analytical basis for failure prediction, Int. J. Fract. 10 (1974) 379−392.
doi: 10.1007/BF00035499

[5] P.N. Sudha, K Sangeetha, K.Jisha, N. Vanisri, Corrosion of ceramic materials fundamental biomaterials: Ceramics, in S. Thomas, P. Balakrishnan, M.S. Sreekala (Eds) (2018) pp. 223–250.
doi: 10.1016/B978-0-08-102203-0.00009-3

[6] M. Ciccotti, Stress-corrosion mechanisms in silicate glasses. J. Phys. D Appl. Phys. 42(21) (2009).

[7] S. Freiman, S.M Wiederhorn, J.J. Mecholsky, Environmentally enhanced fracture of glass: a historical perspective, J. Am. Ceram. Soc. 92 (2009) 1371–1382.
doi: 10.1111/j.1551-2916.2009.03097.x

[8] G.J. Qiao, W. Hongjie, J. Zhihao, Comparison between fatigue behavior of some ceramics: a new concept of intrinsic stress-corrosion exponent n_0, Int. J. Fatigue 24 (2002) 499–508.
doi: 10.1016/S0142-1123(01)00175-X

[9] K.D. Mchenry, E. Richard, R.E. Tressler, High temperature dynamic fatigue of hot pressed SiC and sintered alpha SiC, J. Am. Ceram. Soc. 59(4) (1980) 459–461.

[10] T. Fett, D. Munz, K. Keller, Subcritical crack growth in silicon carbide, J. Mater. Sci. Lett. 16(4) (1997) 324–327.
doi: 10.1023/A:1018573706780

[11] A. Wojteczko, R. Lach, K. Wojteczko, R. Pawel, Subcritical crack growth in oxide and non-oxide ceramics using the constant stress rate test, Proces. App. Ceram. 9(4) (2015) 187–191.
doi: 10.2298/PAC1504187W

[12] J. Lamon, Review: Creep of fibre-reinforced ceramic matrix composites, Int. Mater. Rev. 65 (2019) 28−62.
doi: 10.1080/09506608.2018.1564182

[13] J. Lamon, S. Mazerat, M. R'Mili, Reinforcement of ceramic matrix composites: properties of SiC-based filaments and tows, in P. Narottam, N.P. Bansal, J. Lamon (Eds), Ceramic Matrix Composites: Materials Modelling, and Technology, John Wiley & Sons: Hoboken, NJ, (2015), pp. 3–26.
doi: 10.1002/9781118832998.ch1

[14] S.J. Robertson, M.B. RugglesWrenn, R.S. Hay, T. Shilling, R. Mitchell, B. Kroeger, L. Gumucio, Static fatigue of Hi-Nicalon™-S fiber at elevated temperature in air, steam, and sillicic acid-saturated steam, J. Am. Ceram. Soc. 103(2) (2020) 1358–1371.
doi: 10.1111/jace.16799

[dataset] [15] S. Mazerat, R. Pailler, Statistical data for the tensile properties and static fatigue of SiC-based bundles, Data Brief 32 (2020) 106166.
doi: 10.1016/j.dib.2020.106166

[16] P.L. Swanson, Subcritical crack growth and other time and environment dependent behavior in crustal rocks, J. Geo. Res. 89(B6) (1984) 4137–4152.
doi: 10.1029/JB089iB06p04137

[17] T. Lube, Sub-critical crack growth in alumina – a comparison of different measurement and evaluation methods, BHM 156(11) (2011) 450–456.
doi: 10.1007/s00501-011-0035-y

[18] S.R. Choi, J.A. Salem, N.N. Nemeth, High-temperature slow crack growth of silicon carbide determined by constant-stress-rate and constant-stress testing, J. Mat. Sci. 33 (1998) 1325–1332.
doi: 10.1023/A:1004358516776

[19] N. Al Nasiri, N. Ni, E. Saiz, J. Chevalier, F. Giuliani, L.J. Vandeperre, Effect of microstructure and grain boundary chemistry on slow crack growth in silicon carbide at ambient conditions, J. Eur. Ceram. Soc. 35 (2015) 2253–2260.
doi: 10.1016/j.jeurceramsoc.2015.02.020

[20] S.R. Choi, N.N. Nemeth, J.P. Gyekenyesi, Slow crack growth during static and dynamic loading in silicate glasses, Int. J. Fatigue 28(2) (2006) 164–172.
doi: 10.1016/j.ijfatigue.2005.03.007

[21] T.A. Mihalske, S.W. Freiman, A molecular mechanism for stress corrosion in vitreous silica, J. Am. Ceram. Soc. 66(4) (1983) 284–288.

doi: 10.1111/j.1151-2916.1983.tb15715.x

[22] W. Gauthier, F. Pailler, J. Lamon, R. Pailler, Oxidation of silicon carbide fibers during static fatigue in air at intermediate temperatures, J. Am. Ceram. Soc. 92(9) (2009) 2067−2073.
doi: 10.1111/j.1551-2916.2009.03180.x

[23] C. Laffon, A.M. Flank, P. Lagarde, M. Laridjani, R. Hagege, P. Orly, J. Cotteret, J. Dixier, J.L. Miquel, H. Hommel, A.P. Legrand, Study of Nicalon-based ceramic fibres and powders by EXAFS spectrometry, X-ray diffractometry and some additional methods, J. Mater. Sci. 24 (1989) 1503−1512.
doi: 10.1007/BF02397093

[24] F. Teyssandier, G. Puyoo, S. Mazerat, G. Chollon, R. Pailler, F. Babonneau, Contribution to the understanding of the microstructure of first generation Si-C-O fibers, in: M. Halbig, S. Mathur, T. Ohji, M. Singh (Eds.), Advanced Processing and Manufacturing Technologies for Structural and Multifunctional Materials VI, 33 (2012) of Ceram. Eng. Sci. Proc. Wiley, New York pp. 1–11.
doi: 10.1002/9781118217528.ch1

[25] S. Mazerat, A. Delehouze, R. Pailler, Delayed failure prediction of SiC-based bundles: the impact of sampling size, Int. J. Fatigue 138 (2020) 105694.
doi: 10.1016/j.ijfatigue.2020.105694

[26] W. Gauthier, J. Lamon, Delayed Failure of Hi-Nicalon and Hi-Nicalon S multifilament tows and single filaments at intermediate temperatures (500°-800°C), J. Am. Ceram. Soc. 92(3) (2009) 702−709.
doi: 10.1111/j.1551-2916.2009.02924.x

[27] S. Mazerat, J. Lacroix, B. Rufino R. Pailler, Carbon derived from silicon carbide fibers, a comparative study, Mater. Today Com. 19 (2019) 177–185.
doi: 10.1016/j.mtcomm.2019.01.013

[28] M.E. Ebrahimi, J. Chevalier, G. Fantozzi, Slow crack growth behavior of alumina ceramics, J. Mater. Sci. (1999) 15(1) 142–7.
doi: 10.1557/JMR.2000.0024

[29] C.C. Gonzaga, H.N. Yoshimura, P.F. Cesar, W.G. Miranda, Subcritical crack growth in porcelains, glass-ceramics, and glass-infiltrated alumina composite for dental restorations, J. Mater. Sci: Mater Med 20 (2009) 1017−1024.

doi: 10.1007/s10856-008-3667-z

[30] K. Kumagawa, H. Yamaoka, M. Shibuya, T. Yamamura, Thermal stability and chemical corrosion resistance of newly developed continuous Si-Zr-C-O Tyranno fiber, Ceram. Eng. & Sci. Proceedings 18(3) (1997) 113−118.

doi: 10.1002/9780470294437.ch12

Figure captions

Fig. 1: Endurance diagram comparing the predicted median lifetime (Eq. (2)) for the different fiber types at (a). 600 °C and (b). 800 °C.

Fig. 2: Apparent SCG activation energy versus stress exponent for different SiC-based fiber types. Red triangles and blue dots indicate respectively families ① and ②.

Fig. 3: Evolution of stress exponent with (a). carbon free content or (b). Young modulus.

Fig. 4: Evolution of (a). apparent activation energy for SCG at intermediate temperature with oxygen content and (b). $A^{1/n}$ taken at 600 °C with stress exponent.

Figures

Fig.1

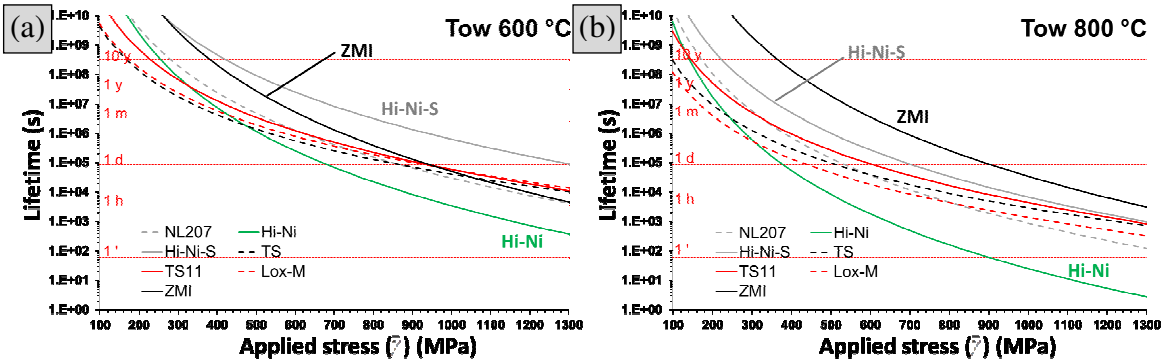

Fig.2

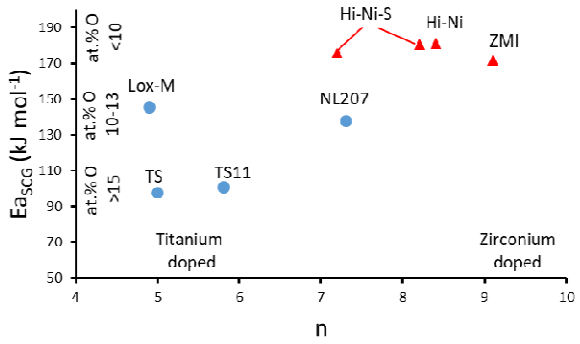
Hi-Ni-S
Hi-Ni
ZMI
Lox-M
NL207
TS
TS11
at.% O <10
at.% O 10-13
at.% O >15
Titanium doped
Zirconium doped
Ea$_{SCG}$ (kJ mol^{-1})
n
190
170
150
130
110
90
70
50
4
5
6
7
8
9
10

Fig.3

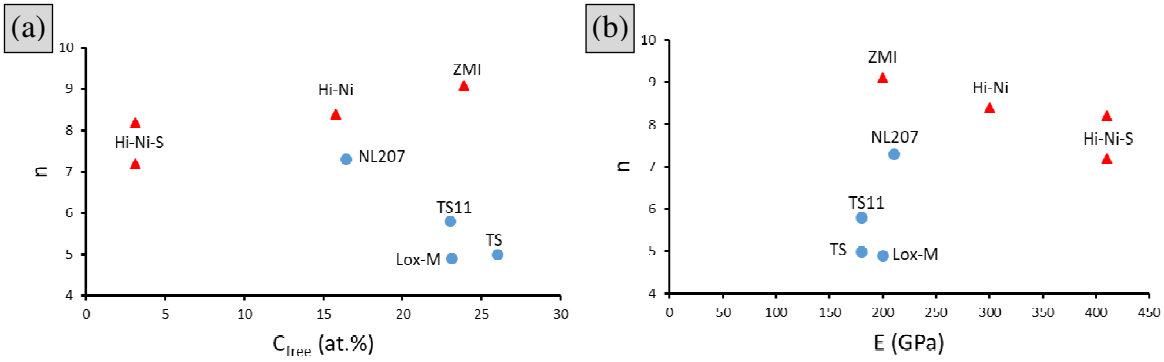
(a)
n
C_{free} (at.%)
Hi-Ni-S
Hi-Ni
ZMI
NL207
TS11
TS
Lox-M
(b)
n
E (GPa)
ZMI
Hi-Ni
NL207
Hi-Ni-S
TS11
TS
Lox-M

Fig.4

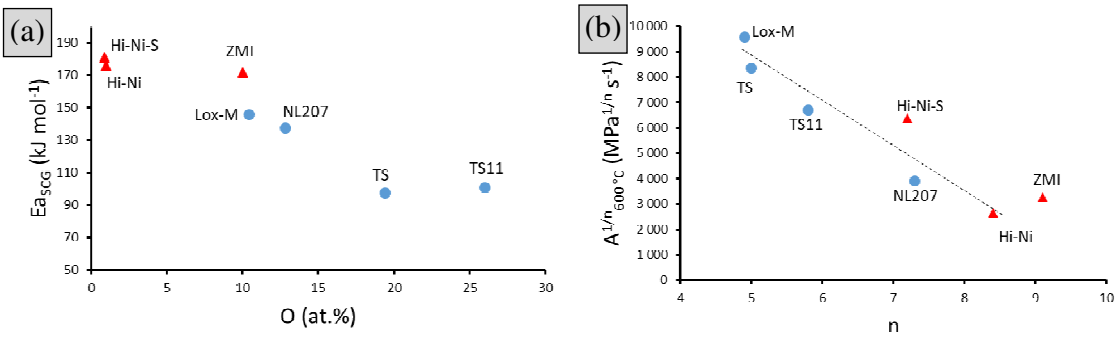
(a)
Hi-Ni-S
Hi-Ni
ZMI
Lox-M
NL207
TS
TS11
Ea$_{SCG}$ (kJ mol^{-1})
O (at.%)
(b)
Lox-M
TS
TS11
Hi-Ni-S
NL207
ZMI
Hi-Ni
A$^{1/n}_{600°C}$ (MPa$^{1/n}$ s^{-1})
n

Table captions

Table 1: Composition, physical and mechanical properties completed with SCG parameters for the different SiC-based fibers.

Table 1

	NL207	TS	TS11	Lox-M	ZMI	Hi-Ni	Hi-Ni-S
Si	38.6	31.8	31.6	35.4	35.5	41.9	48.2
C	48.6	48.1	41.7	53.3	54.3	57.2	50.8
O (at.%)	12.8	19.4	26.0	10.4	10.0	0.9	1.0
other	-	(Ti) 0.7	(Ti) 0.7	(Ti) 0.9	(Zr) 0.2	-	-
C_{free}	16.4	26.0	23.0	23.1	23.9	15.8	3.1
Grain size (nm)	1.9	1.2	1.2	1.9	2.2	5.0	50
K_{IC} (MPa $m^{1/2}$)	1.20	1.11	1.12	1.11	1.01	1.66	1.86
E (GPa)	210	180	180	200	200	300	410
n	7.3	5.0	5.8	4.9	9.1	8.4	7.2
$A_{500\,°C}$ (MPa s^n)	2.0×10^{27}	2.4×10^{20}	9.4×10^{22}	4.3×10^{20}	2.1×10^{33}	1.5×10^{30}	5.7×10^{28}
$A_{600\,°C}$ (MPa s^n)	1.7×10^{26}	4.1×10^{19}	1.6×10^{22}	3.2×10^{19}	9.8×10^{31}	5.8×10^{28}	2.5×10^{27}
$A_{700\,°C}$ (MPa s^n)	2.4×10^{25}	1.0×10^{19}	3.7×10^{21}	4.1×10^{18}	8.6×10^{30}	4.5×10^{27}	2.1×10^{26}
$A_{800\,°C}$ (MPa s^n)	5.0×10^{24}	3.3×10^{18}	1.2×10^{21}	7.6×10^{17}	1.2×10^{30}	5.5×10^{26}	2.7×10^{25}
Ea_{SCG} (kJ mol^{-1})	140	100	100	150	170	180	170
A_0 (MPa s^n)	9.8×10^{17}	5.8×10^{13}	1.4×10^{16}	6.1×10^{10}	5.1×10^{21}	8.4×10^{17}	7.3×10^{16}